Environmental Science and Ecotechnology 30 (2026) 100680

Contents lists available at ScienceDirect

Environmental Science and Ecotechnology

journal homepage: www.journals.elsevier.com/environmental-science-and-ecotechnology/

Original Research

Phenolic contaminants generate persistent phenoxyl radicals to accelerate antibiotic degradation

Liping Luo [a], Shiqing Zhou [b], Jianfei Zhou [c], Jingquan Wang [a], Han Wu [a], Hongguang Guo [a,c,*]

[a] State Key Laboratory of Intelligent Construction and Healthy Operation and Maintenance of Deep Underground Engineering, College of Architecture and Environment, Sichuan University, Chengdu, 610065, China
[b] Hunan Engineering Research Centre of Water Security Technology and Application, College of Civil Engineering, Hunan University, Changsha, 410082, China
[c] Key Laboratory of Leather Chemistry and Engineering (Sichuan University), Ministry of Education, Chengdu, 610065, China

ARTICLE INFO

Article history:
Received 8 July 2025
Received in revised form
25 February 2026
Accepted 26 February 2026

Keywords:
Interactions between contaminants
Phenoxyl radicals
Chlorite
Mn(VII)

ABSTRACT

Water pollution by coexisting multiple contaminants presents escalating challenges to environmental remediation and public health protection. In advanced oxidation processes, contaminant interactions are invariably regarded as detrimental, introducing competitive reactions and matrix interferences that diminish treatment efficiency. However, phenolic compounds—a prevalent class of recalcitrant water pollutants—possess latent oxidative capabilities that remain strategically unexploited. Whether their reactivity can be harnessed to accelerate, rather than impede, the removal of priority contaminants remains fundamentally unclear. Here we show that in the permanganate/chlorite (Mn(VII)/ClO_2^-) system, phenolic compounds undergo a counterintuitive transformation into persistent phenoxyl radicals that enhance sulfamethoxazole degradation by 3.5- to 20-fold. Mechanistic investigations reveal that these radicals exhibit exceptional stability and selectivity, preferentially attacking target pollutants while demonstrating robust resistance to common matrix interferences—properties unattainable with conventional oxidants alone. Quantitative structure-activity relationships provide predictive frameworks for optimizing this contaminant-assisted oxidation strategy across diverse chemical scenarios. This contaminant-mediated oxidation strategy inverts the traditional paradigm of mutual interference, transforming recalcitrant phenolics from obstacles into powerful mediators. The findings open new avenues for self-adaptive remediation of multi-pollutant systems and suggest broader applications in environmental cleanup where contaminant interactions can be strategically exploited.

1. Introduction

Global water scarcity, exacerbated by contamination from emerging contaminants (ECs), such as persistent organic pollutants and antibiotics, has reached crisis levels in vulnerable regions [1,2]. For decades, direct adsorption and advanced oxidation processes (AOPs) have been indispensable strategies [3–8]. Of these strategies, AOPs have attracted greater attention due to their inherent destructive capacity and advantages in avoiding secondary treatment. Typically, these processes generate high-potential radicals (•OH, E_0 = 1.9–2.7 V_{NHE}; $SO_4^{\bullet-}$, E_0 = 2.5–3.1 V_{NHE}) that attack and degrade ECs, where NHE stands for the normal hydrogen electrode. [7–10]. However, complex matrices often sabotage these processes [11–14] due to the indiscriminate attack characteristics of these active species [15]. Finally, their decontamination performance in real waters often falls short of laboratory expectations.

In complex water matrices, the coexistence of multiple contaminants poses a critical yet underexplored challenge. This oversight stems from the prevailing assumption that ECs are intrinsically inactive toward one another and act only as competitors for reactive species. A recent study found that the coexistence of phenol and naphthol in a UV–vis-activated Mn(II) process

* Corresponding author. State Key Laboratory of Intelligent Construction and Healthy Operation and Maintenance of Deep Underground Engineering, College of Architecture and Environment, Sichuan University, Chengdu, 610065, China.
E-mail address: hgguo@scu.edu.cn (H. Guo).

https://doi.org/10.1016/j.ese.2026.100680

slightly accelerates naphthol degradation, challenging the prevailing assumption [16]. In the literature, the positive effect of phenol on non-naphthol is limited. This gives rise to several questions. Is this positive effect pollutant selective, or does it have general applicability when coexisting with other non-phenolic pollutants? Is this positive effect controllable and scalable? Elucidating the mechanisms underlying this positive effect and its role in promoting pollutant degradation across diverse coexistence systems, including nonphenolic targets and mixtures of various pollutant types, may provide valuable insights into these questions. Yet such studies remain scarce.

Our previous work on the Mn(VII)/chlorite system uncovered a proton-coupled electron transfer (PCET) mechanism within ternary contaminant–Mn–chlorite complexes, in which the contaminant structure dictates reactivity [17]. Herein, we hypothesize that coexisting pollutants may actively engage in the reaction network. To test this, sulfonamide pollutants (SAs), an important category of ECs widely present in water bodies, were selected as representative non-phenolic target pollutants, and the Mn(VII)/chlorite process is used as a representative oxidation process. This study addresses three pivotal aspects: (1) the degradation performance of SAs by the Mn(VII)/chlorite process in the presence or absence of ECs; (2) the hidden roles of PCs-derived intermediates; and (3) the development of quantitative structure–activity relationships (QSARs) between various PCs and ECs to assist in predicting and rationally utilizing this interaction.

2. Materials and methods

2.1. Reagents

All chemicals used in this study are listed in Supplementary Text S1. The chemical properties and structures of the studied contaminants are provided in Supplementary Table S1.

2.2. Experimental methods

The degradation performance of contaminants by the Mn(VII)/chlorite process, with or without PCs, was examined in a batch reactor. The initial solution pH was adjusted with phosphate buffer (Supplementary Fig. S1). A glass vessel was initially filled with a solution containing 3 μmol L^{-1} SAs along with the target PCs. Subsequently, 50 μmol L^{-1} chlorite and 30 μmol L^{-1} Mn(VII), the optimal concentration explored in our previous study, were sequentially introduced to initiate the reaction [17]. At predetermined time intervals, 1 mL of the sample was taken, immediately quenched with an excess of thiosulfate, and then filtered for LC quantitative analysis. All experiments were performed in duplicate at least twice to ensure reproducibility, and the error bars represent the standard deviation.

2.3. Analytical and theoretical calculation methods

Analytical details are provided in Supplementary Text S2 and Table S2. Density functional theory (DFT) calculations were performed using the Gaussian 16 rev. C.01 program and molecular dynamics [18]. Geometries were optimized, and vibrational frequencies were obtained at the B3LYP level, followed by single-point energy refinements using B3LYP-D3(BJ)/6-311++G (d,p). Solvent effects were evaluated using the Integral Equation Formalism Polarizable Continuum Model. Thermodynamic data were calculated using the Shermo software [19].

3. Results and discussion

3.1. Degradation performance of contaminants under various systems

3.1.1. A comprehensive assessment of the coexistence impact of different contaminants during the Mn(VII)/chlorite process

In our previous study, we found that the Mn(VII)/chlorite process exhibits excellent removal of SAs, which are widely detected in natural waters [20]. SMX was selected as a model contaminant to examine the influence of the coexistence of different contaminants on the decontamination effect of the Mn(VII)/chlorite process. The coexistence of the most commonly explored contaminants significantly inhibited or even halted SMX degradation (Supplementary Fig. S2), which could be attributable to the predictable competitive effects of these contaminants on reactive species in the Mn(VII)/chlorite process. Surprisingly, adding bisphenol A (BPA) dramatically accelerated SMX degradation, with the removal rate approaching 100% within 5 min, compared with approximately 15% without BPA.

3.1.2. Differentiated facilitative role of PCs in contaminant removal

To elucidate the promoting effect of PCs on SMX degradation in the Mn(VII)/chlorite system, a series of structurally simple PCs with varying para-substituents, including p-cresol (MP), 4-methoxyphenol (MOP), 4-chlorophenol (4-CP), phenol (PE), 4-hydroxyacetophenone (HAP), para-hydroxybenzaldehyde (HBAl), methyl p-hydroxybenzoate (MeP), 4-hydroxybenzoic acid (HBAc), and hydroquinone (HQ), were selected for systematic evaluation. Except for HQ (discussed later), the selected PCs accelerated SMX degradation by Mn(VII)/chlorite to varying degrees, exceeding rates observed without PCs by approximately 3.5–20-fold (Fig. 1a and Supplementary Fig. S3). Notably, the negligible oxidation of SMX observed in all control experiments confirmed that the enhancement was not attributed to the direct reactions of phenols with Mn(VII) or chlorite but rather to a synergistic interaction among the three components (i.e., PCs, Mn(VII), and chlorite, Supplementary Fig. S4). The reasons for selecting phenolic concentrations of 50 μmol L^{-1} are shown in Supplementary Text S3 and Fig. S5. Kinetically, the degradation of SMX followed pseudo-first-order kinetics, regardless of the presence or absence of PCs (Supplementary Fig. S6).

Moreover, the analogous PCs-accelerated effect was not observed in widely studied AOPs, such as ferrous ion/hydrogen peroxide (Fe^{2+}/H_2O_2), ferrous ion/peroxymonosulfate (Fe^{2+}/PMS), or Mn(VII)/bisulfite (Mn(VII)/HSO_3^-) processes (Supplementary Fig. S7), indicating a distinctive role of PCs in the oxidation of contaminants via the Mn(VII)/chlorite process.

3.2. Identification of reactive species in PCs-induced accelerated oxidation

To clarify the reaction mechanism underlying the PCs-induced acceleration of SMX degradation in the Mn(VII)/chlorite process, traditional reactive intermediates, including reactive oxygen species (ROS) and reactive Mn species (RMnS), were first examined.

3.2.1. Exclusion of PCs-induced production of reactive oxygen species

It is well accepted that the phenolic hydroxyl group can mediate the formation of reactive oxygen species—hydroxyl radicals (OH•), superoxide radicals ($O_2^{\bullet-}$), and singlet oxygen ($^1O_2$)—through electron and proton transfer with oxidants in basic redox processes or catalysis in natural soils and AOPs for water decontamination [21,22]. Electron paramagnetic resonance (EPR)

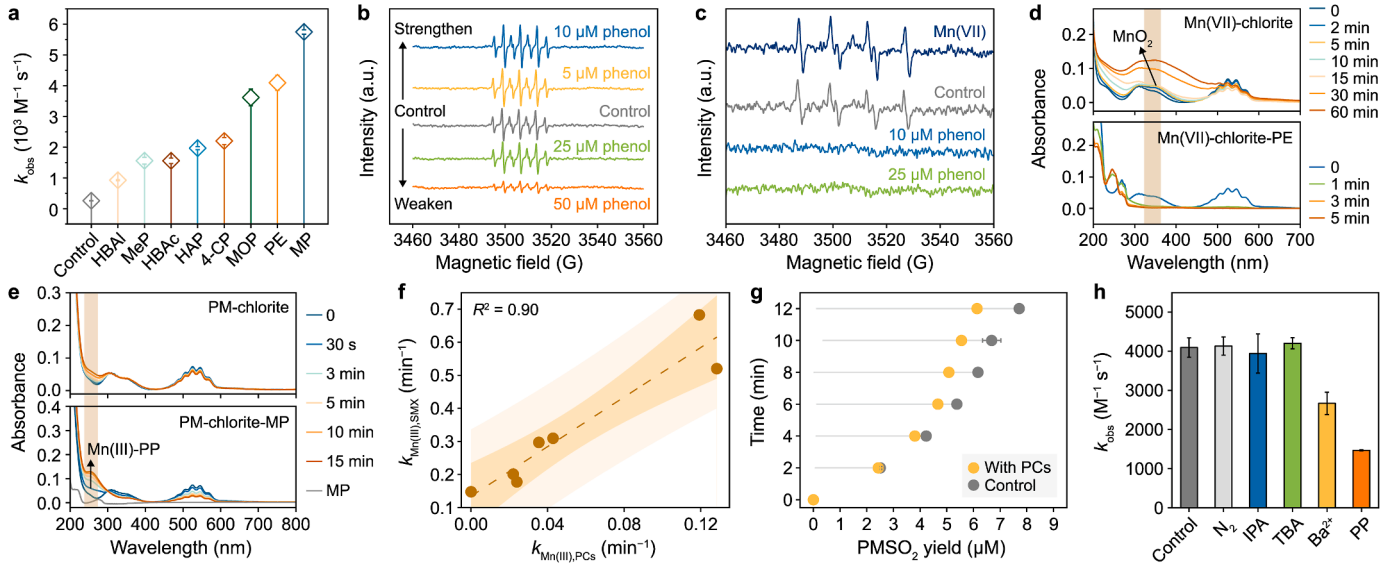

Fig. 1. Phenolic compounds promote SMX degradation in the Mn(VII)–chlorite **system. a**, Degradation of sulfamethoxazole (SMX) by Mn(VII)/chlorite process in the presence of varying phenol compounds (PCs). **b**,**c**, DMPO-probed ESR spectra of Mn(VII)-chlorite in the presence of varying concentration phenol in water (**b**) and in dimethyl sulfoxide (**c**). **d**, Ultraviolet-visible (UV–vis) spectra of Mn(VII)/chlorite system with and without PCs. **e**, UV–vis spectra of Mn(VII)/chlorite with and without PCs under excess pyrophosphate (PP). **f**, Relationship between the oxidation reactivities of Mn(III) towards SMX and PCs in the PCs–Mn(VII)–chlorite system. Shaded areas represent the 95% confidence (darker) and prediction (lighter). **g**, Methyl phenyl sulfone ($PMSO_2$) yields in the Mn(VII)/chlorite process with and without PCs. **h**, Effects of scavengers on SMX removal in the Mn(VII)/chlorite process in the presence of PCs. DMPO: 5,5-dimethyl-1-pyrroline N-oxide; UV–vis spectra: ultraviolet-visible spectra; MP: p-cresol; MOP: 4-methoxyphenol; 4-CP: 4-chlorophenol; PE: phenol; HAP: 4-hydroxyacetophenone; HBAl: para-hydroxybenzaldehyde; MeP: methyl p-hydroxybenzoate; HBAc: 4-hydroxybenzoic acid; IPA: isopropanol; TBA: tert-butanol; PM: Mn(VII).

spectroscopy with 5,5-dimethyl-1-pyrroline N-oxide (DMPO) as a spin-trapping agent is commonly used to detect these species [23]. DMPO was directly oxidized to DMPO-OX (oxidized 5,5-dimethyl-1-pyrroline N-oxide), exhibiting an intensity ratio of 1:2:1:2:1:2:1 (Fig. 1b) [17], indicating strong or moderate oxidation in the Mn(VII)/chlorite process [24]. In the presence of PCs, the signal intensity of DMPO-OX increased at lower concentrations but decreased at higher PCs concentrations in the Mn(VII)/chlorite system. Notably, a concentration-dependent biphasic trend of the DMPO-OX signal was in marked contrast to SMX degradation, which showed continuous acceleration throughout the tested PCs concentration range (0–500 μmol L^{-1}, Supplementary Fig. S5). This indicates that the changes in the DMPO-OX signal is not a reliable indicator for the evaluation of HO• production. In addition, the negligible effect of tert-butyl alcohol (TBA) as a quencher ($k_{•OH,TBA} = (3.8–7.8) \times 10^8$ M^{-1} s^{-1}) [25] on SMX abatement roughly supported the irrelevant effects of HO• (Fig. 1h).

Furthermore, to provide more accurate information about HO•, $O_2^{•-}$ detection can be applied as an indirect indicator for the presence of HO•, as they are usually associated [13]. The spectra of $O_2^{•-}$ were recorded in dimethyl sulfoxide solvent to improve the stability of $O_2^{•-}$ and prevent interference from HO• [23,26]. The characteristic 5,5-dimethyl-1-pyrroline N-oxide–hydroperoxyl radical adduct (DMPO-•OOH) signals, with an intensity ratio of 1:1:1:1 (Fig. 1c), assigned to $O_2^{•-}$ were identified in the Mn(VII) alone system, which is consistent with a previous study [27]. This is possibly because Mn(VII) directly oxidizes DMPO or Mn(VII) transforms dissolved oxygen into $O_2^{•-}$, which is then protonated to form hydroperoxyl radicals (•OOH) [27]. Oxidative species from O_2 can be excluded based on the negligible influence of N_2 and O_2 purging—which removes dissolved oxygen or adds dissolved oxygen—on SMX degradation (Fig. 1h and Supplementary Fig. S8). In addition, the DMPO-•OOH intensity decreased upon the addition of chlorite and disappeared completely after the continued addition of PCs (Fig. 1c), suggesting that neither HO• nor $O_2^{•-}$ is an active intermediate responsible for enhanced SMX degradation by PCs in the Mn(VII)-chlorite process. Moreover, no $^1O_2$ generation was detected when using 2,2,6,6-tetramethyl-4-piperidinyloxyl (TEMP) as the spin-trapping agent for $^1O_2$ (Supplementary Fig. S9). In addition, multiple lines of evidence suggest that chlorine-related species (chlorine dioxide (ClO_2), hypochlorite radical (•OCl), chlorine radical (•Cl), dichloride radical ($•Cl_2^-$), etc.) are almost certainly irrelevant to the PCs-accelerated effect (Supplementary Text S4; Fig. 1b–h; and Supplementary Fig. S10–S12).

3.2.2. *Role of Mn(VII)-derived intermediates (RMnS)*

To further elucidate the PCs-accelerated effect in the Mn(VII)/chlorite system, the depletion behavior of Mn(VII) was examined under different conditions. The residual Mn(VII) concentration was determined by measuring the solution's absorbance at 525 nm. In the absence of PCs, the Mn(VII) concentration gradually decreased during the reaction, with a decay rate constant (k_{decay}) of 0.04 min^{-1} (Supplementary Fig. S13). Remarkably, PCs significantly enhanced Mn(VII) consumption, increasing k_{decay} to 0.21–2.49 min^{-1}, following the order MP > 4-CP > PE > HAP > HBHc > MeP > HBAl. Except for MOP (data not shown), the order of varying PCs-induced acceleration of Mn(VII) depletion was largely consistent with that of SMX degradation induced by different PCs in Mn(VII)/chlorite process (Fig. 1a). This implies that the roles of the Mn(VII) reduction products—Mn(III), Mn(V), Mn(VI), and manganese dioxide (MnO_2), which have been widely reported as potential candidates for reactive intermediate–enhancing contaminant oxidation in Mn(VII)-based AOPs [28], which need to be comprehensively elucidated.

Ultraviolet-visible (UV-vis) spectra, a powerful tool often used to detect manganese-related substances, are applied in this section to comprehensively elucidate Mn(VII) reduction products [24,29]. The evolution of the UV-vis spectra of the Mn(VII)/chlorite process at 200–800 nm in the absence or presence of PCs (Fig. 1d). Obviously, as the reaction progressed, the peak at 525 nm

decreased, and a new peak at 370 nm formed, which intensified over time. The distinctive absorbance peaks at 525 and 370 nm were identified as Mn(VII) and colloidal MnO_2, respectively (Supplementary Fig. S14). This indicates that Mn(VII) was reduced by chlorite to colloidal MnO_2 [17,30]. Nevertheless, no characteristic peak associated with MnO_2 was detected when PCs were added to the Mn(VII)/chlorite process (Fig. 1d and Supplementary Fig. S15), indicating that PCs altered the chemical behavior of manganese in the system or rapidly transformed MnO_2 into other species. The latter can be excluded by the slow kinetics of PCs in the *ex situ*-prepared MnO_2 colloidal solution, where Mn(VII) is reduced by chlorite (Supplementary Text S5 and Fig. S16).

Pyrophosphate (PP), a specific ligand for Mn(III), forms a stable Mn(III)–PP complex with an absorbance peak at 258 nm, enabling spectroscopic detection [24]. To prevent interference from external PCs on characteristic peaks at 250–260 nm, MP was selected as the model to record UV-vis spectra during the reaction in the Mn(VII)/chlorite process in the absence or presence of MP at excessive PP doses (Fig. 1e). The results show that without MP, the reduction of Mn(VII) by chlorite generated a small amount of Mn(III), as evidenced by a weak absorption band at 258 nm. Remarkably, the introduction of MP significantly strengthened the characteristic peak at 258 nm and decreased the peak at 525 nm compared with the Mn(VII)/chlorite system, indicating that MP significantly enhanced Mn(VII) depletion and Mn(III) generation. A similar phenomenon was found in the presence of other PCs (Supplementary Text S6 and Fig. S17). To further determine the roles of the produced Mn(III), PP inhibition experiments were performed due to the redox inertness of the Mn(III)-PP complex [17]. The increased PP concentration (from 0 to 5 mM) partially hindered SMX degradation in the PCs–Mn(VII)–chlorite system from $(4.10 \pm 0.25) \times 10^3$ M^{-1} s^{-1} to $(1.47 \pm 0.01) \times 10^3$ M^{-1} s^{-1} (Fig. 1h), suggesting the important role of Mn(III) in SMX direct oxidation or the induction of actual active species, which was also found in other PCs-accelerated systems (Supplementary Fig. S18).

To further investigate the role of Mn(III), the rate constants of Mn(III) with PCs ($k_{Mn(III),PCs}$) and SMX ($k_{Mn(III),SMX}$) were examined in various PCs–Mn(VII)–chlorite systems (for details, see Supplementary Text S7). The contributions of Mn(III) to SMX are highly positively correlated with those to PCs (fitting correlation coefficient $R^2 > 0.9$, Fig. 1f), implying that PCs have a considerable potential to compete with SMX for Mn(III) consumption. That is, if Mn(III) acts as the direct oxidant of SMX in the PCs-coexisting system, the faster reaction kinetics of Mn(III) with PCs will result in its faster competitive consumption of Mn(III) (Supplementary Fig. S19), ultimately inhibiting SMX degradation, as observed in other systems (Supplementary Fig. S7). Nevertheless, this proposal contradicts the experimental results of PCs-accelerated SMX degradation (Supplementary Fig. S3). Therefore, compared with directly oxidizing SMX, Mn(III) is more likely responsible for inducing the production of the actual active species in the Mn(VII)/chlorite process under PCs-coexisting conditions.

According to a previous study, barium ions (Ba^{2+}) can act as a quencher agent for Mn(V) and Mn(VI) by precipitating Mn(VI) (K_{sp} ($BaMnO_4$) $= 2.5 \times 10^{-10}$ M^{-1} s^{-1}) [31]. The k_{obs} of SMX degradation decreased from $(4.10 \pm 0.25) \times 10^{-3}$ M^{-1} s^{-1} to $(2.67 \pm 0.28) \times 10^{-3}$ M^{-1} s^{-1} with the Ba^{2+} concentration increased from 0 to 10 mM in the Mn(VII)/chlorite process in the presence of PE (Fig. 1h and Supplementary Fig. S20), demonstrating that Mn(VI)/Mn(V) may play an indispensable role in this system. On the other hand, due to a lack of available Mn(V) quenchers, relatively stable Mn(V) and Mn(VI) were prepared to independently investigate the oxidation of SMX by Mn(V)/Mn(VI) in the presence of PCs (for details, see Supplementary Text S8) [28,32]. To maintain consistency, chlorite was added to each system. The presence of PCs significantly enhanced SMX degradation by Mn(V), whereas the stable Mn(VI) was inert to SMX, regardless of the presence of chlorite or PCs (Supplementary Fig. S21–S22). Thus, the quenching of Ba^{2+} is likely ascribed to the limited production of Mn(V) by precipitating Mn(VI) (equation (1)).

Since Mn(V) tends to undergo spontaneous disproportionation under experimental conditions (pH = 4.7, equations (1) and (2)), making it extremely unstable [28], UV-vis spectra failed to provide evidence. To further reveal the interaction between PCs and Mn(V), methyl phenyl sulfoxide (PMSO) was used as a probe. According to equations (3) and (4), since MeP is inert with Mn(VII) and chlorite (Supplementary Fig. S4), it can affect the formation of methyl phenyl sulfone ($PMSO_2$) only by reacting with Mn(VI)/Mn(V). Thus, MeP was used as the model to evaluate the effect of PCs on Mn(VI)/Mn(V). The presence of PCs slowed down the transformation of PMSO to $PMSO_2$ remarkably over time (Fig. 1g), suggesting that their presence fails to induce Mn(VI)/Mn(V) production but rather consumes them in the Mn(VII)-chlorite process.

Based on the above evidence, it is reasonable to conclude that Mn(V) acts as a key reactive intermediate reacting with PCs to induce a specific active species to degrade SMX rather than directly oxidize SMX.

$$2Mn(VI) \rightarrow Mn(VII) + Mn(V)\ (\text{disproportionation}) \quad (1)$$

$$2Mn(V) \rightarrow Mn(VI) + Mn(IV)\ (\text{disproportionation}) \quad (2)$$

$$Mn(VII) + PMSO \rightarrow Mn(V) + PMSO_2 \quad (3)$$

$$Mn(V) + PMSO \rightarrow Mn(III) + PMSO_2 \quad (4)$$

3.2.3. Identification of long-lived species: phenoxyl radicals

As discussed earlier, the presence of PCs in the Mn(VII)/chlorite process leads to the formation of unknown active species that enhance SMX removal. To examine this, PCs, chlorite, and Mn(VII) were premixed for 60 min to complete the induction stage (forming the unknown active species) and eliminate interference from the transient intermediates Mn(V) and Mn(III). SMX was then added to initiate the subsequent degradation stage. Surprisingly, upon addition of SMX, it degraded rapidly and was completely removed within 3 min (Fig. 2a). Notably, no residual Mn(VII) was detected in the system after the induction phase (Supplementary Fig. S23). Meanwhile, there was no significant difference in chlorite concentration before and after SMX degradation (Supplementary Fig. S24). These results imply that the removal of SMX during the degradation phase depends solely on a long-lived reactive species produced during the induction phase, rather than on catalytic oxidation by Mn(VII) or chlorite. More convincingly, a cyclic experiment demonstrated that the long-lived active intermediate is produced only when Mn(VII), chlorite, and PCs coexist (Supplementary Text S9 and Fig. 2b). This evidence suggests that focusing on the degradation of PCs—another important component of the ternary system—in the Mn(VII)/chlorite process may be conducive to identifying the unknown active species responsible for SMX degradation.

The degradation of PCs exhibited varying degrees of delayed kinetics (Supplementary Fig. S25), which may be ascribed to differences in the physicochemical properties of the various substituents on the benzene ring of PCs [33]. Interestingly, SMX degradation in the presence of the corresponding PCs showed highly synchronized, delayed evolution (yellow lines in Supplementary Fig. S3). Furthermore, the delayed effects of PCs

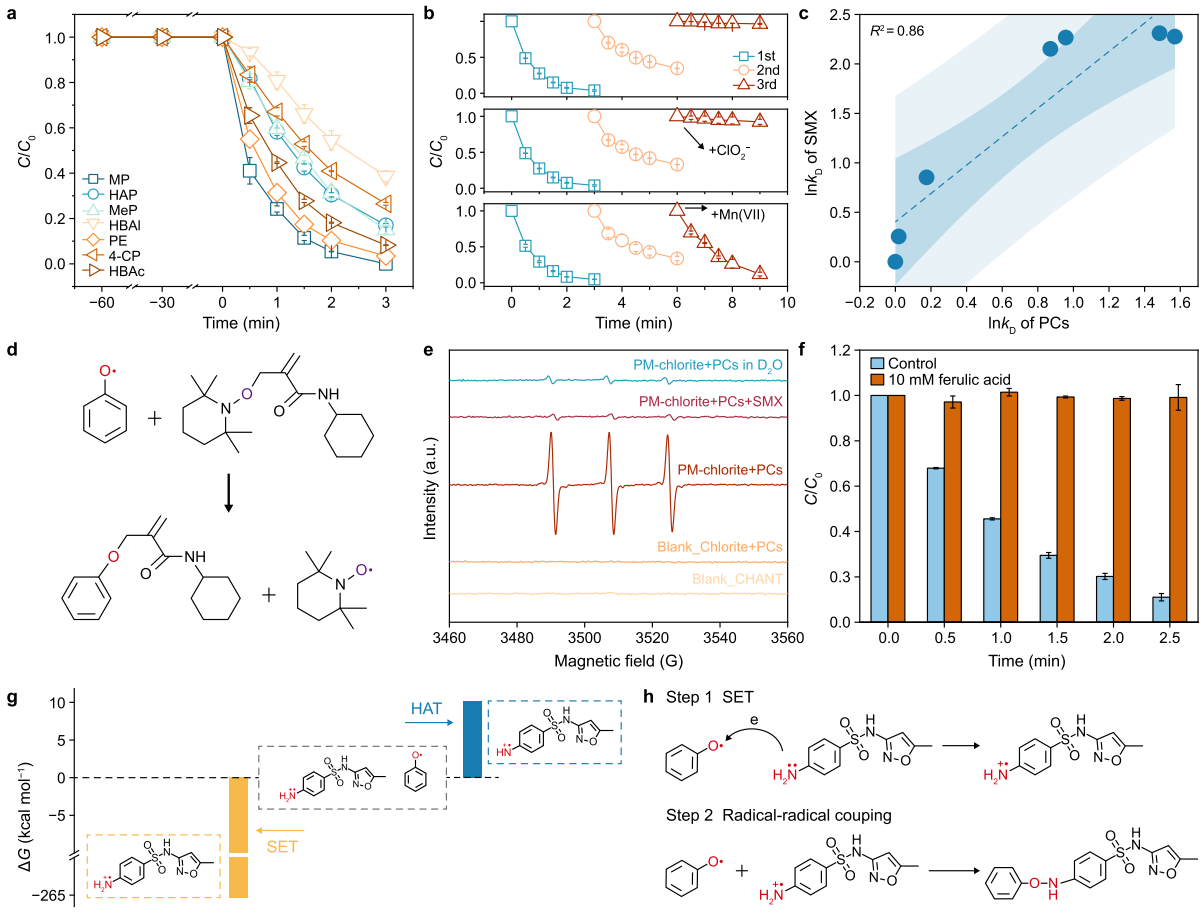

Fig. 2. Evidence for phenoxyl-radical involvement in PCs–Mn(VII)–chlorite oxidation. **a**, Sulfamethoxazole (SMX) degradation in PCs–Mn(VII)–chlorite systems after the induction stage. Data are mean ± standard deviation. **b**, SMX degradation by PE–Mn(VII)–chlorite in cycle experiment. 1st, 2nd, and 3rd: the first, second, and third additions of SMX to the reaction system. The three panels from top to bottom show systems after adding: SMX only, ClO_2^- and SMX, and Mn(VII) and SMX, respectively. The black arrow indicates the addition point. **c**, Correlation between $\ln k_D$ of SMX and $\ln k_D$ of PCs in PCs–Mn(VII)–chlorite systems. Data are mean ± standard deviation. Shaded areas represent the 95% confidence (darker) and prediction (lighter). **d**, Trapping mechanism of phenoxyl radicals by CHANT. **e**, Electron paramagnetic resonance spectra for the reaction product when CHANT trapps phenoxyl radicals in different systems. **f**, Effect of ferulic acid on SMX degradation in PE–Mn(VII)–chlorite system. **g**, Gibbs free energy of single-electron transfer and hydrogen atom transfer steps between SMX and phenoxyl radical. **h**, Transformation pathways of SMX by phenoxyl radical. PCs: phenol compounds; CHANT: (2,2,6,6-tetramethylpiperidin-1-yl) oxyl (TEMPO)-based traps containing alkyl; MP: p-cresol; MOP: 4-methoxyphenol; 4-CP: 4-chlorophenol; PE: phenol; HAP: 4-hydroxyacetophenone; HBAl: para-hydroxybenzaldehyde; MeP: methyl p-hydroxybenzoate; HBAc: 4-hydroxybenzoic acid; PM: Mn(VII); HAT: hydrogen atom transfer; SET: single-electron transfer; $\ln k_D$: Quantification of delayed reaction kinetics.

and SMX removal in various systems were quantified as a $\ln k_D$ index based on a unified definition (Supplementary Text S10). In the presence of PCs, the ln*k*D of SMX abatement was highly linearly related to that of the corresponding PCs ($R^2 > 0.8$; Fig. 2c). Moreover, the $\ln k_{obs}$ of SMX were obviously negatively correlated with the $\ln k_D$ of the corresponding PCs in the PCs–Mn(VII)–chlorite processes (Supplementary Fig. S26). Therefore, it is reasonable to speculate that the PCs-accelerated degradation of SMX is strongly associated with the PCs' oxidized products during this process.

Phenoxyl radicals are widely recognized as key intermediates in phenol oxidation [34–36], yet their direct detection remains difficult due to their low reactivity. To address this, Yu et al. developed a trapping agent (2,2,6,6-tetramethylpiperidin-1-yl) oxyl (TEMPO)-based traps containing the alkyl (CHANT) trapping method, which generates two detectable products: a persistent TEMPO radical monitored by EPR and a cross-coupled stable adduct identified by ultraperformance liquid chromatography–mass spectrometry (UPLC–MS) [37]. A schematic diagram of the capture mechanism is shown in Fig. 2d. In this study, both products were detected when CHANT was used to trap phenoxy radicals. The typical triplet peaks of TEMPO persistent radicals, released by CHANT reacting with phenoxyl radicals, appeared in the presence of PCs in the Mn(VII)/chlorite process (Fig. 2e). Meanwhile, another cross-coupled stable adduct from CHANT-trapped phenoxyl radicals was also detected by UPLC–MS with $(M + H)^+/Z$ of 260.17 (Supplementary Fig. S27). Furthermore, ferulic acid (FA), known to quench phenoxyl radicals by converting them back to inert phenols [38], completely inhibited SMX degradation when applied after the induction stage (Fig. 2f and Supplementary Fig. S28).

Together, the CHANT trapping (EPR and MS evidence) and FA inhibition results provide a consistent line of evidence for the involvement of a phenoxyl radical in PCs–Mn(VII)–chlorite processes (Supplementary Fig. S29).

Moreover, the addition of excess EDTA before the degradation stage, which can complex with Mn species [39], completely inhibited SMX degradation by phenoxyl radicals (Supplementary Fig. S30), indicating that the complexation of Mn species plays a critical role in the long life of phenoxyl radicals.

3.3. Reaction mechanism of phenoxyl radicals in contaminant oxidation

To determine how phenoxyl radicals react with SMX, structurally SMX-related substructural compounds were examined after the complete induction period. Structurally, SMX consists of an aniline ring and a five-membered heterocyclic N-containing ring with methyl groups connected via a sulfonamide bond. Aniline (AN), sulfanilamide (SAM), and 3-amino-5-methylisoxazole (AMI) were selected as the substructure compounds to investigate the reactive site in SMX toward phenoxyl radicals. AN and SAM exhibited higher reactivity toward phenoxyl radicals with k_{obs} of $(3.38 \pm 0.77) \times 10^3$ and $(1.36 \pm 0.08) \times 10^3$ M^{-1} s^{-1}, while the k_{obs} of AMI was only $(1.47 \pm 0.03) \times 10^1$ M^{-1} s^{-1} (Supplementary Fig. S31), suggesting that the aniline site, rather than the heterocyclic N-containing ring, serves as the primary reactive site in SMX. Moreover, the PCs-acceleration effect has been observed with other pollutants containing amino groups but not with those lacking an amino group (Supplementary Fig. S32).

Previous studies have indicated that phenoxyl radicals and SAs may form two reaction products—Michael adducts and radical–radical coupling products—resulting from the delocalization of the phenoxyl radical's unpaired electron [40–42]. The former reaction was excluded from this study (for details, see Supplementary Text S11 and Fig. S33). HPLC−MS was employed to identify the transformation products of SMX during the degradation phase (after induction) to further understand the reaction mechanism. A major product with a molecular ion at m/z 346.09, observed at 4.2 min, was detected (Supplementary Fig. S34), consistent with typical radical–radical coupling products [43]. These findings provide additional evidence of the formation of phenoxyl radicals in the Mn(VII)/chlorite system in the presence of PCs. Furthermore, our investigation did not detect any intermediate fragments associated with conventional SMX degradation pathways, such as hydroxylation, oxidation, coupling, or bond cleavage (Supplementary Table S3 and Fig. S34–S35).

In the radical–radical coupling process, the generation of sulfonamide radicals (i.e., $SMX^{\bullet+}$ or $SMX\text{-}H^{\bullet+}$) is the critical premise. Commonly, sulfonamide radicals are produced by single-electron transfer (SET) and hydrogen atom transfer (HAT) reactions between SMX and phenoxyl radicals, similar to the previously described reaction between SMX and organic radicals (i.e., semiquinone radicals and acetylperoxyl radicals) [41,43]. The two formation steps of sulfonamide radicals require further differentiation. Due to the lack of direct experimental approaches, DFT was applied to elucidate the reaction mechanism based on the thermodynamic feasibility of the two initial steps (Fig. 2g). The Gibbs free energies of HAT and SET were +10.19 and −265.33 kcal mol^{-1}, respectively, which means that SET is thermodynamically favorable, while HAT is not.

3.4. Generation mechanism of phenoxyl radicals

3.4.1. Experimental insights

As discussed above, SMX removal depends on the oxidative conversion of PCs to phenoxyl radicals in the PCs-coexistence system. Generally, PCs with strong electron-donating properties tend to react faster with oxidants [13]. Interestingly, we observed an unusual “inverted V-shaped” dependence of k_{obs} on the electron-donating ability, as described by the Hammett constant (σ^+), across varying PCs (Fig. 3a).

Our previous studies have indicated that contaminant oxidation in the Mn(VII)/chlorite system occurs via a unique PCET mechanism in which electrons are transferred across hydrogen bonds (TEHB) in a hydrogen-bonded adduct involving the contaminants, Mn(VII), and chlorite [17]. Given that replacing water (H_2O) with deuterium oxide (D_2O) impairs proton-coupled reactions, we conducted several solvent-exchange experiments to further investigate this effect [44]. As expected, replacing H_2O with D_2O completely inhibited SMX removal in the presence of all investigated PCs; however, the PCs themselves remained partially degraded (Fig. 3b and Supplementary Fig. S36). This suggests that D_2O replacement does not inhibit SMX removal by completely preventing the degradation of PCs but rather by disrupting the TEHB-mediated conversion of PCs into phenoxyl radicals. The EPR signal of CHANT trapping phenoxyl radicals decreased remarkably in D_2O solvent, providing conclusive evidence for the hindered generation of phenoxyl radicals in D_2O solvent (Fig. 2e).

Further kinetic experiments were conducted at different pH values (pH 5–9) to provide further evidence of the role of proton activity (Supplementary Fig. S37). In these experiments, the degradation efficiency of SMX decreased sharply with increases in pH, and the reaction was completely inhibited at pH 9. Evidently, the key step in the TEHB process is the formation of a hydrogen bond (H-bond), which is typically sensitive to ionic strength and is easily disturbed by changes in ionic strength in the working solution [45]. Our investigation of the effect of ionic strength on SMX degradation and Mn(VII) depletion in each PCs–Mn(VII)–chlorite system suggests that an increase in perchlorate concentration from 0 to 200 mM greatly suppressed SMX degradation and Mn(VII) depletion, again corroborating this interaction (Supplementary Fig. S38–S39). Together, it can be concluded that phenoxyl radical generation proceeds via a TEHB reaction within a ternary H-bond complex comprising PCs, Mn(VII), and chlorite. Under the examined conditions (pH ≈ 4.7), the phenolic groups of PCs are expected to remain ($pK_a > 9$), maintaining proton availability for the TEHB process.

3.4.2. Calculation insights

To elucidate the mechanism of the ternary hydrogen-bond complex responsible for generating phenoxyl radicals, DFT calculations were performed to examine its intrinsic coordination structure. Phenol was selected as a representative substrate, and three plausible configurations of phenol, Mn(VII), and chlorite were proposed (Fig. 3c): hydrogen bonding between phenolic H and chlorite-double bond O (configuration 1), phenolic H and Mn(VII) O (configuration 2), and phenolic H and chlorite single-bond O (configuration 3). Of these, configuration 1 was identified as the most probable structure due to its lowest relative energy (Supplementary Table S4).

From the perspective of molecular orbital theory, electron transfer occurs spontaneously from the highest unoccupied molecular orbital (HOMO) of the electron donor to the lowest unoccupied molecular orbital (LUMO) of the electron acceptor. A smaller energy gap between these orbitals typically results in a faster reaction rate [46,47]. The electronic structures of the HOMO and LUMO energy levels explain the “inverted V-shaped” trend observed before (Fig. 3d and Supplementary Table S5). Specifically, the LUMO energy of Mn(VII) (the electron acceptor) was −3.84 eV. For the electron donors, the HOMO energies (E_{HOMO}) of MOP and HQ (−5.70 and −5.79 eV, respectively) were higher than that of chlorite (−5.81 eV), whereas the HOMO energies of other PCs were lower. This indicates that PCs with a lower E_{HOMO} than chlorite undergo interfacial electron tunneling via chlorite-mediated hydrogen bonds, ultimately producing phenoxyl radicals for SMX degradation. In contrast, PCs with a higher E_{HOMO} than chlorite exhibit strong electron-donating ability, directly donating electrons to Mn(VII) and thereby consuming Mn(VII) inefficiently. As a result, the higher electron-donating MOP and HQ exhibit lower PCs-accelerated effects on SMX degradation in the Mn(VII)/chlorite process.

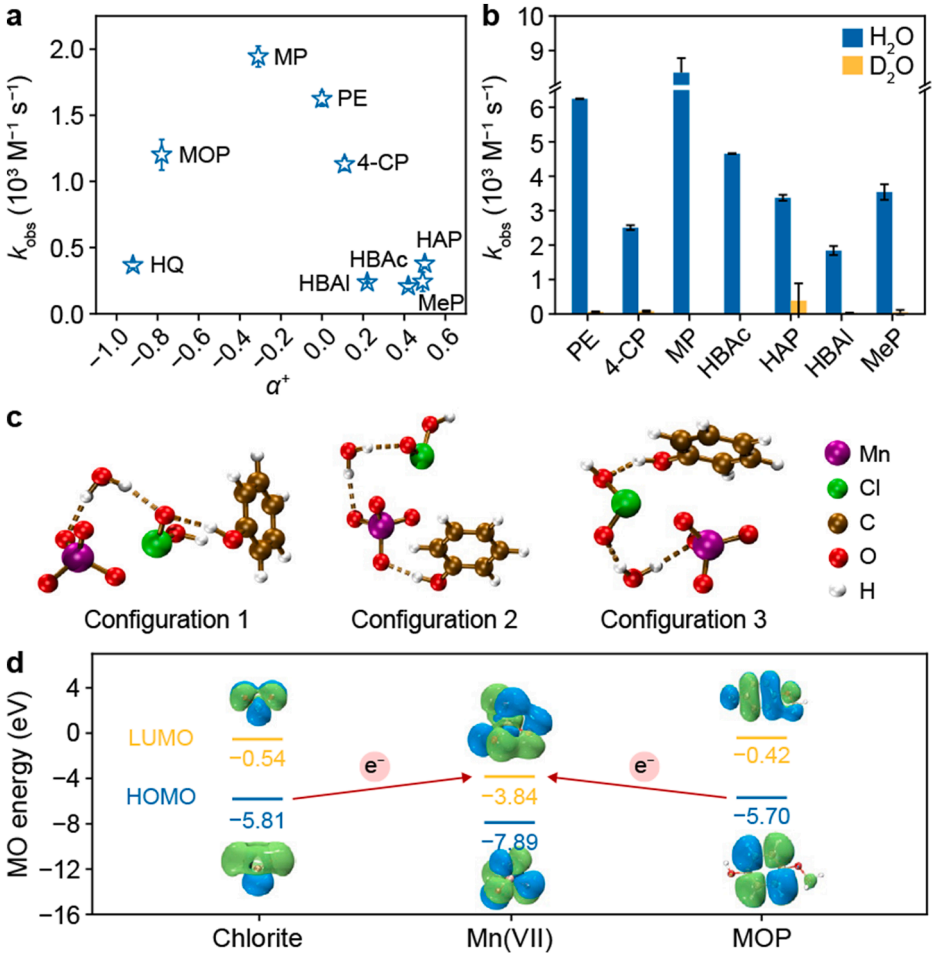

Fig. 3. Proton activity and hydrogen bonding govern TEHB-mediated phenoxyl-radical f**ormation. a**, Dependence of the observed sulfamethoxazole (SMX) degradation rate constant (k_{obs}) on the Hammett substituent constant (σ^+) of phenol compounds (PCs) across PCs–Mn(VII)–chlorite systems under low PCs concentration (10 μmol L^{-1}). Data are mean ± standard deviation. **b**, Effect of using D_2O to replace solvents H_2O on SMX degradation in PCs–Mn(VII)–chlorite system. Data are mean ± standard deviation. **c**, Optimized structure models of three possible conformations of phenol, Mn(VII), and chlorite. **d**, Comparison of the highest unoccupied molecular orbital energy (HOMO) and lowest unoccupied molecular orbital energy (LUMO) among Mn(VII), chlorite, and 4-methoxyphenol (MOP); MP: p-cresol; MOP: 4-methoxyphenol; 4-CP: 4-chlorophenol; PE: phenol; HAP: 4-hydroxyacetophenone; HBAl: para-hydroxybenzaldehyde; MeP: methyl p-hydroxybenzoate; HBAc: 4-hydroxybenzoic acid; MO: molecular orbital; configuration 1: hydrogen bonding between phenolic H and chlorite-double bond O; configuration 2: between phenolic H and the O of Mn(VII); configuration 3: phenolic H and the single-bonded O of chlorite.

From a thermodynamic perspective, we conducted DFT calculations to determine the Gibbs free energies using MnO_4^- and chlorite as proton acceptors. The results showed that the ΔG value for the phenol reaction in the Mn(VII)/chlorite system with chlorite as the proton acceptor (−2.18 kcal mol^{-1}) was considerably more favorable than that without chlorite (ΔG = 6.26 kcal mol^{-1}, indicating a nonspontaneous reaction). This result confirms that the generation of phenoxy radicals (from PCs with a lower E_{HOMO} than chlorite) occurs through a PCET reaction mediated by chlorite. Given the similarity between HAT and PCET, spin density analysis further supports the PCET mechanism (Supplementary Text S12, Fig. S40, and Table S6).

3.5. Demystifying the dynamic process of PCs reshaping EC removal

According to the above discussion, the mechanism of PCs-accelerated effects on SMX degradation in the Mn(VII)/chlorite process involves two aspects (Scheme 1): the generation of new reactive phenoxyl radicals and the acceleration of Mn(III) formation. Specifically, chlorite acts as a hydrogen bond acceptor

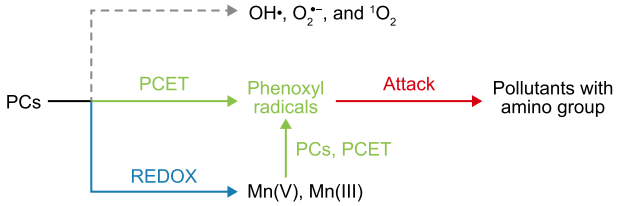

Scheme 1. Proposed mechanism of phenol compounds (PCs)-enhanced degradation in the Mn(VII)–chlorite process. PCET: proton-coupled electron transfer.

through its oxygen atoms, forming hydrogen bonds with the hydroxyl hydrogen donors of phenols. Upon the introduction of Mn(VII), a new ternary H-bond complex reactive center (PCs–ClO_2^-–Mn(VII)*) is formed for a preliminary PCET reaction, leading to the generation of phenoxyl radicals and reactive manganese species (RMnS, (Mn(V)/Mn(III)). Moreover, chlorite serves as a reductant, reducing Mn(VII) to RMnS. The generated RMnS, acting similarly to Mn(VII), functions as a component of the ternary reaction center (PCs–ClO_2^-–Mn(V)*/Mn(III)), initiating the

secondary PCET reaction. This was responsible for the characteristic delayed response when certain PCs with low electron-donating properties accelerated the degradation of SMX (Supplementary Fig. S3). Finally, the presence of PCs converted the active intermediates in the system from short-lived RMnS to long-lived phenoxyl radicals. Subsequently, the produced phenoxyl radicals followed a two-step process to remove SMX. That is, phenoxyl radicals grasped one electron from the N site in the aniline moiety of SMX to first produce SMX•$^+$. Subsequently, a rapid SMX degradation was achieved via radical-radical coupling between phenoxyl radicals and the SMX•$^+$ produced (Fig. 2h).

3.6. Production and selective performance of phenoxyl radicals

3.6.1. The key to phenoxyl radical production

Elucidating the mechanism of phenoxyl radical production is key to understanding the law governing the acceleration of SMX degradation by PCs with different para-substituents. During the phenoxyl radical generation process (PCET), proton transfer (PT) typically involves O–H bond cleavage, and the corresponding O–H bond dissociation energies (BDEs) vary notably with the nature of the substituent due to conjugation effects (Supplementary Table S5). As expected, these BDEs exhibited a strong linear correlation with the lnk_{obs} of SMX degradation in the corresponding PCs–Mn(VII)–chlorite systems, with an R^2 of 0.84 (Fig. 4a). Further, the lnk_{obs} of SMX degradation in varying PCs–Mn(VII)–chlorite systems strongly correlated with pK_a (a key descriptor associated with PT), with an R^2 value of up to 0.98, which is consistent with the previous PT process (Fig. 4b) [48]. These findings suggest that, as the pK_a of a PC approaches the working-solution pH, a larger fraction of the PC exists in its deprotonated form, which is more detrimental to SMX degradation. Accordingly, the PCs-induced acceleration effect is highly correlated with the PCs form in solution [49,50]. Therefore, the form of PCs is strongly responsible for the production of phenoxyl radicals in the PCs-Mn(VII)-chlorite system.

3.6.2. Insight into the selective oxidation of phenoxyl radicals

Premixing PCs, chlorite, and Mn(VII) for 60 min provided an ideal environment for examining the oxidation selectivity of phenoxyl radicals toward different representative SAs with different molecular structures. Phenoxyl radical exerted differential decomposition behaviors on these SAs (Supplementary Fig. S41). We then applied QSAR analysis to assess the relationships between phenoxyl radical reactivities and the structural properties of SAs. We selected appropriate molecular descriptors, including the dissociation constant (pK_a), E_{HOMO}, and octanol–water partition coefficient (K_{ow}), as they are widely used to characterize the physicochemical properties of organic compounds in water treatment research [13]. Details regarding the sources of these descriptors are provided (Supplementary Text S13). The results showed that electronic features and proton-transfer ability did not dominate the selective oxidation of SAs by phenoxyl radicals, as evidenced by low correlations of approximately 0.1 and 0.6 (Supplementary Text S14 and Fig. S42).

In contrast, lnk_{obs} was strongly and linearly correlated with K_{ow} (R^2 = 0.8; Fig. 4c). This correlation is noteworthy because K_{ow}, which reflects the hydrophobicity of a compound, is not usually implicated in the selective oxidation of contaminants by inorganic active species, such as high-valent metals [13] or oxidant complexes [51]. In general, a higher K_{ow} indicates that a compound is more hydrophobic. Our results, therefore, suggest that phenoxyl radical–mediated oxidation exhibits a unique hydrophobicity-driven selectivity.

Mechanistically, this can be rationalized by considering the steric hindrance of phenoxyl radicals. Unlike small inorganic oxidants, which attack contaminants mainly through direct collision, phenoxyl radicals are bulkier, and their accessibility to sulfonamides becomes a key determinant of reactivity. Hydrophobic interactions between the aromatic ring of phenoxyl radicals and the hydrophobic regions of sulfonamides help bring the radicals into closer proximity to the active sites of the contaminant. This interaction facilitates overlap with the unpaired electrons of the radicals, thereby accelerating electron transfer and controlling the reaction rate. In simple terms, the more hydrophobic the sulfonamide, the more strongly it interacts with phenoxyl radicals, and the more readily it undergoes oxidation.

3.7. Effect of water constituents and real waters on phenoxyl radical reactivity

Inorganic anions (such as NO_3^-, SO_4^{2-}, and Cl^-) and humic acid (HA), common coexisting ions and a major component of natural organic matter in real wastewater, typically hinder contaminants' removal in the water treatment process [52]. We investigated the effects of NO_3^- (0–10 mM), SO_4^{2-} (0–10 mM), Cl^- (0–10 mM), and HA (0–10 mg L^{-1}) on SMX abatement after completing the induction stage. Both inorganic anions and natural organic matter hardly affected the degradation of SMX by phenoxyl radicals (Fig. 4d), which indicates that phenoxyl radicals have excellent resistance to water matrix interference. Moreover, the effects of real water on SMX abatement after completing the induction stage were also estimated (Fig. 4d). Quality parameters of the tested actual water were listed in Supplementary Table S7. Phenoxyl

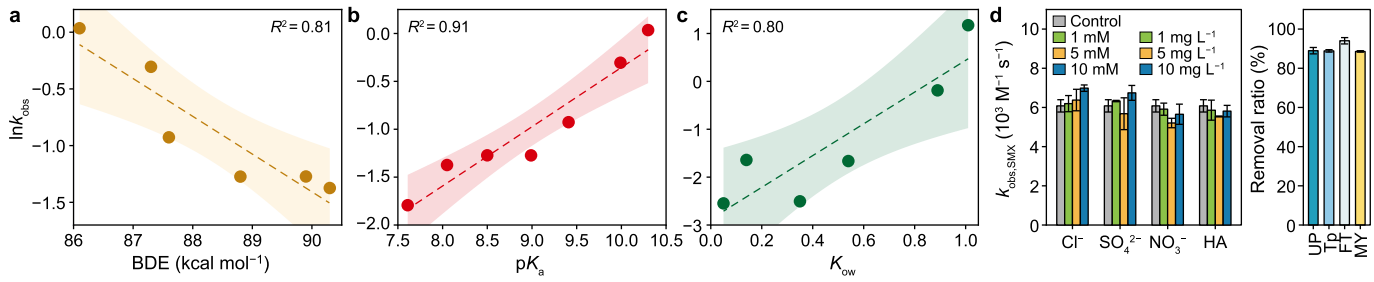

Fig. 4. Structure–reactivity relationships and matrix effects for phenoxyl-radical oxidation. a,**b**, Correlations between lnk_{obs} of sulfamethoxazole (SMX) degradation and bond dissociation energies (BDE; (**a**) and acid dissociation constant (pK_a; **b**) of phenol compounds (PCs) in PCs–Mn(VII)–chlorite process. **c**, Correlation between lnk_{obs} of sulfonamide pollutants (SAs) and their octanol–water partition coefficient (K_{ow}) in phenol (PE)–Mn(VII)–chlorite process. The shaded areas in panels a, b, and c represent the 95% confidence intervals. **d**, Effects of water matrix (left) and real water samples (right) on SMX degradation by phenoxyl radical. Left: k_{obs} of SMX degradation in the presence of Cl^-, SO_4^{2-}, NO_3^- (1–10 mM), and humic acid (HA, 1–10 mg L^{-1}). Right: SMX removal ratio in ultrapure water (UP), tap water (Tp), fountain water (FT), and Mingyan Lake water (MY). Data are mean ± standard deviation.

radicals exhibited good reactivity in real water samples, such as tap water (88.9%), fountain water (94.0%), and freshwater from Mingyuan Lake (88.6%).

4. Conclusion

A comprehensive assessment of the coexistence and interactions among contaminants in oxidation processes, and the elucidation of their intrinsic mechanisms, are vital for the rational application of advanced water treatment technologies. Using SMX as a model, this study first conducted a comprehensive evaluation of how coexisting contaminants affect the degradation of the target compound in the Mn(VII)/chlorite process. Subsequently, we conducted an in-depth exploration of the prominent positive effects of PCs. It was found that PCs with lower E_{HOMO} than chlorite exhibit remarkable activated amplification effects (3.5–20-fold), mediated by PCET pathways that convert RMnS into long-lived phenoxyl radicals. Remarkably, these radicals exhibit exceptional advantages, including extended half-life, substrate selectivity (K_{ow}-dependent targeting), and robust resistance to the complex matrices of background substances (adding inorganic anions and real waters). Moreover, the generation of phenoxyl radicals depends primarily on the pK_a of PCs, and their reactivity is closely related to the K_{ow} of the target contaminants, providing theoretical insights for future applications of these long-lived phenoxyl radicals.

This study indicates that phenol-assisted oxidation can enhance the removal of sulfonamide antibiotics in Mn(VII)/chlorite systems, making pharmaceutical wastewater—where phenolic byproducts and sulfonamides often coexist—a promising application scenario. For practical engineering implementation, a Mn(VII)/chlorite pre-oxidation unit can be integrated as a front-end treatment stage upstream of conventional biological processes in pharmaceutical wastewater plants to remove sulfonamides and enhance the biodegradability of various pollutants for subsequent treatment. The process operates under mild conditions with moderate chemical requirements and can be controlled by monitoring phenolic compound levels to enable appropriate oxidant dosing. While the phenol-assisted oxidation process shows promising results in the laboratory, its practical implementation in real-world systems poses several challenges. One significant challenge is precisely quantifying the concentrations of both phenolic compounds and sulfonamides in wastewater, as fluctuations in their levels can affect treatment efficiency. In addition, seasonal and compositional fluctuations in wastewater characteristics may affect process stability and parameter fine-tuning. These issues highlight the need for adaptive control systems, potentially coupled with machine learning–based predictive algorithms, to optimize the treatment process in real time. Moreover, integrating the Mn(VII)/chlorite pre-oxidation unit with downstream biological systems requires monitoring oxidants, such as permanganate and chlorite, as high concentrations may inhibit microbial activity and reduce biological treatment efficiency. Therefore, further research should focus on optimizing the process parameters, addressing these operational challenges, and conducting pilot-scale tests to better understand the system's viability for large-scale applications. Overall, this work provides a theoretical basis for the development of AOPs, from treating water matrices as passive media to actively designing contaminant coexistence networks to enhance water decontamination.

CRediT authorship contribution statement

Liping Luo: Writing – review & editing, Writing – original draft, Methodology, Investigation, Formal analysis, Conceptualization. **Shiqing Zhou:** Validation, Investigation. **Jianfei Zhou:** Resources. **Jingquan Wang:** Methodology. **Han Wu:** Software. **Hongguang Guo:** Writing – review & editing, Validation, Supervision, Resources, Project administration, Funding acquisition.

Declaration of competing interest

The authors declare that they have no known competing financial interests or personal relationships that could have appeared to influence the work reported in this paper.

Acknowledgments

The authors would like to thank the National Key Research and Development Program of China (2023YFC3210100), National Natural Science Foundation of China (52470107), and Sichuan Science and Technology Program (2023NSFSC1949) for the financial support.

Appendix A. Supplementary data

Supplementary data to this article can be found online at https://doi.org/10.1016/j.ese.2026.100680.

References

[1] C. Gao, H. He, W. Qiu, Y. Zheng, Y. Chen, S. Hu, X. Zhao, Oxidative stress, endocrine disturbance, and immune interference in humans showed relationships to serum bisphenol concentrations in a dense industrial area, Environ. Sci. Technol. 55 (2021) 1953–1963.
[2] K. Kaetzl, M. Riegel, B. Joseph, R. Ossenbrink, H. Gerber, W. Gwenzi, T. Morck, D. Laner, T. Heinrich, V. Kromrey, K. Friedrich, M. Wachendorf, K. Stenchly, Biogenic activated carbons from conservation grassland biomass for organic micropollutants removal in municipal wastewater, Environ. Sci. Ecotechnol. 26 (2025) 100588.
[3] M. Bouzidi, N. Alwadai, M. Al Huwayz, R. Tronco, M. de Oliveira, T. da Rosa Salles, T. Saidani, F. Nunes, B. Westermann, S. Fagan, C. Ramos, L. Silva, G. Dotto, C. Rhoden, Efficient removal of organophosphate insecticide employing magnetic chitosan-derivatives, Int. J. Biol. Macromol. 279 (2024) 134992.
[4] F. da Silva Bruckmann, J. Gonçalves, L. Silva, M. Oliveira, G. Dotto, C. Rhoden, Chitosan-based adsorbents for wastewater treatment: a comprehensive review, Int. J. Biol. Macromol. 309 (2025) 143173.
[5] F. Nunes, F. da Silva Bruckmann, A. Viana, T. da Rosa Salles, L. Zancanaro, D. Rhoden, C. Franco, A.P. Schuch, G.L. Dotto, L. Silva, C. Ramos, C. Rhoden, Removal of selective serotonin reuptake inhibitor using magnetic graphene oxide derivatives: adsorption study in low drug concentration using HPLC quantification, in vitro safety, and phytotoxicity, J, Environ. Chem. 12 (2024) 112336.
[6] A. Rubim, J. Rubenick, L. Vendrame, I. Zanella, C. Rolim, C. Rhoden, Formulation and characterization of amiodarone-methyl-beta-cyclodextrin inclusion complexes: a molecular modelling perspective, J. Mol. Graphics Modell. 126 (2024) 108639.
[7] J. Lee, U. von Gunten, J. Kim, Persulfate-based advanced oxidation: critical assessment of opportunities and roadblocks, Environ. Sci. Technol. 54 (2020) 3064–3081.
[8] L. Li, X. Qian, S. Wang, Y. Liu, D. Wang, H. Zhang, Y. An, H. Cheng, J. Ma, Unveiling non-radical oxidation pathways in peroxymonosulfate/cobalt(II) systems: critical role of cobalt(III) and cobalt(IV) explored by manganese(II) probing, J. Hazard. Mater. 495 (2025) 139014.
[9] J. Wang, S. Wang, Reactive species in advanced oxidation processes: formation, identification and reaction mechanism, Chem. Eng. J. 401 (2020) 126158.
[10] Y. Liu, N. Du, X. Liu, D. Yao, D. Wu, Z. Li, S. Mao, ZnS-embedded porous carbon for peroxydisulfate activation: enhanced electron transfer for bisphenol A degradation, Environ. Sci. Ecotechnol. 19 (2024) 100338.
[11] Z. Cao, X. Yu, Y. Zheng, E. Aghdam, B. Sun, M. Song, A. Wang, J. Han, J. Zhang, Micropollutant abatement by the UV/chloramine process in potable water reuse: a review, J. Hazard. Mater. 424 (2022) 127341.
[12] T. Vo, J. Rintala, L. Dai, W. Oh, C. He, The role of ubiquitous metal ions in degradation of microplastics in hot-compressed water, Water Res. 245 (2023) 120672.
[13] J. Wang, Z. Chai, H. Su, E. Du, X. Guan, H. Guo, Unraveling the role of humic acid in the oxidation of phenolic contaminants by soluble manganese oxo-Anions, Environ. Sci. Technol. 58 (2024) 8576–8586.
[14] S. Peng, L. Yu, M. Shen, S. Lin, Y. Ye, F. Zhu, J. Xu, J. Pawliszyn, G. Ouyang, Identification of omitted pollutants in environmental water via in situ thin-

film microextraction, Anal. Chem. 96 (2024) 15387–15393.
[15] X. Duan, H. Sun, Z. Shao, S. Wang, Nonradical reactions in environmental remediation processes: uncertainty and challenges, Appl. Catal. B Environ. 224 (2018) 973–982.
[16] X. Wang, W. Xiang, S. Wang, J. Ge, R. Qu, Z. Wang, Oxidative oligomerization of phenolic endocrine disrupting chemicals mediated by Mn(III)-L complexes and the role of Phenoxyl radicals in the enhanced removal: experimental and theoretical studies, Environ. Sci. Technol. 54 (2020) 1573–1582.
[17] L. Luo, M. Zheng, E. Du, J. Wang, X. Guan, H. Guo, Development of a new Permanganate/chlorite process for water decontamination, Environ. Sci. Technol. (2024).
[18] M.J. Frisch, G. Trucks, H. Schlegel, G.E. Scuseria, M. Robb, J. Cheeseman, G. Scalmani, V. Barone, G.A. Petersson, H. Nakatsuji, X. Li, M. Caricato, A. Marenich, J. Bloino, B. Janesko, R. Gomperts, B. Mennucci, H.P. Hratchian, J. Ortiz, A. Izmaylov, J.L. Sonnenberg, Williams, F. Ding, F. Lipparini, F. Egidi, J. Goings, B. Peng, A. Petrone, T. Henderson, D. Ranasinghe, V. Zakrzewski, J. Gao, N. Rega, G. Zheng, W. Liang, M. Hada, M. Ehara, K. Toyota, R. Fukuda, J. Hasegawa, M. Ishida, T. Nakajima, Y. Honda, O. Kitao, H. Nakai, T. Vreven, K. Throssell, J. Montgomery Jr., J. Peralta, F. Ogliaro, M.J. Bearpark, J. Heyd, E. Brothers, K. Kudin, V. Staroverov, T. Keith, R. Kobayashi, J. Normand, K. Raghavachari, A. Rendell, J. Burant, S. Iyengar, J. Tomasi, M. Cossi, J. Millam, M. Klene, C. Adamo, R. Cammi, J. Ochterski, R. Martin, K. Morokuma, O. Farkas, J. Foresman, D. Fox, Gaussian 16 Rev. C.01, in, Wallingford, CT2016.
[19] T. Lu, Q. Chen, Shermo: a general code for calculating molecular thermochemistry properties, Comput. Theor. Chem. 1200 (2021) 113249.
[20] Q. Zhang, G. Ying, C. Pan, Y. Liu, J. Zhao, Comprehensive evaluation of antibiotics emission and fate in the river basins of China: source analysis, multimedia modeling, and linkage to bacterial resistance, Environ. Sci. Technol. 49 (2015) 6772–6782.
[21] L. Pospíšilová, E. Horáková, M. Fišera, M. Jerzykiewicz, L. Menšík, Effect of selected organic materials on soil humic acids chemical properties, Environ. Res. 187 (2020) 109663.
[22] A. Bhandari, F. Xu, Impact of peroxidase addition on the sorption−desorption behavior of phenolic contaminants in surface soils, Environ. Sci. Technol. 35 (2001) 3163–3168.
[23] J. Fontmorin, R. Burgos Castillo, W. Tang, M. Sillanpää, Stability of 5,5-dimethyl-1-pyrroline-N-oxide as a spin-trap for quantification of hydroxyl radicals in processes based on fenton reaction, Water Res. 99 (2016) 24–32.
[24] T. Yang, J. Mai, M. Zhu, Q. Peng, C. Huang, S. Wu, Q. Tan, J. Jia, J. Fang, J. Ma, Enhanced permanganate activation under UVA-LED irradiation: unraveled mechanism involving manganese species and hydroxyl radical, Environ. Sci. Technol. 56 (2022) 17720–17731.
[25] R. Su, N. Li, Z. Liu, X. Song, W. Liu, B. Gao, W. Zhou, Q. Yue, Q. Li, Revealing the generation of high-valent cobalt species and chlorine dioxide in the Co_3O_4-Activated chlorite process: insight into the proton enhancement effect, Environ. Sci. Technol. 57 (2023) 1882–1893.
[26] G. Buettner, On the reaction of superoxide with DMPO/*OOH, Free Radic Res Commun. 10 (1990) 11–15.
[27] K. Xu, H. Dong, M. Li, Z. Qiang, Quinone group enhances the degradation of levofloxacin by aqueous permanganate: kinetics and mechanism, Water Res. 143 (2018) 109–116.
[28] Y. Gao, Y. Zhou, S. Pang, J. Jiang, Z. Yang, Y. Shen, Z. Wang, P. Wang, L. Wang, New insights into the combination of permanganate and bisulfite as a novel advanced oxidation process: importance of high valent manganese-oxo species and sulfate radical, Environ. Sci. Technol. 53 (2019) 3689–3696.
[29] Y. Zhou, Y. Gao, J. Jiang, Y. Shen, S. Pang, Y. Song, Q. Guo, A comparison study of levofloxacin degradation by peroxymonosulfate and permanganate: kinetics, products and effect of quinone group, J. Hazard. Mater. 403 (2021) 123834.
[30] L. An, X. Xu, F. Yan, W. Du, R. Dai, Simultaneous removal of Cyanobacteria and algal organic matter by Mn(VII)/CaSO3 enhanced coagulation: performance and mechanism, J. Hazard. Mater. 485 (2025) 136839.
[31] J. Chen, B. Sun, Y. Zhu, Y. Yang, X. Guan, Unraveling the role of Mn(VI) and Mn(V) species in contaminant abatement by permanganate, Environ. Sci. Technol. Lett. 9 (2022) 446–451.
[32] A. Carrington, M.C.R. Symons 655, Structure and reactivity of the oxy-anions of transition metals. Part I. The manganese oxy-anions, J. Chem. Soc. (1956) 3373–3380.
[33] J. Laszakovits, A. Kerr, A. MacKay, Permanganate oxidation of organic contaminants and model compounds, Environ. Sci. Technol. 56 (2022) 4728–4748.
[34] L. Liu, Q. Liu, Y. Wang, J. Huang, W. Wang, L. Duan, X. Yang, X. Yu, X. Han, N. Liu, Nonradical activation of peroxydisulfate promoted by oxygen vacancy-laden NiO for catalytic phenol oxidative polymerization, App, Catal. B: Environ. Times 254 (2019) 166–173.
[35] S. Remke, T. Bürgin, L. Ludvíková, D. Heger, O.S. Wenger, U. von Gunten, S. Canonica, Photochemical oxidation of phenols and anilines mediated by phenoxyl radicals in aqueous solution, Water Res. 213 (2022) 118095.
[36] D. Šmejkalová, A. Piccolo, M. Spiteller, Oligomerization of Humic phenolic monomers by oxidative coupling under biomimetic catalysis, Environ. Sci. Technol. 40 (2006) 6955–6962.
[37] H. Liu, X. Shu, M. Huang, B. Wu, J. Chen, X. Wang, H. Li, H. Yu, Tailoring d-band center of high-valent metal-oxo species for pollutant removal via complete polymerization, Nat. Commun. 15 (2024) 2327.
[38] A. Amić, Z. Marković, J.M. Dimitrić Marković, D. Milenković, V. Stepanić, Antioxidative potential of ferulic acid phenoxyl radical, Phytochemistry 170 (2020) 112218.
[39] J. Summers, J. Baker, D. Meyerstein, A. Mizrahi, I. Zilbermann, H. Cohen, C. Wilson, J. Jones, Measured rates of fluoride/metal association correlate with rates of superoxide/metal reactions for FeIII-EDTA(H_2O)- and related complexes, J. Am. Chem. Soc. 130 (2008) 1727–1734.
[40] A. Alsoufi, M. Altarawneh, B.Z. Dlugogorski, E.M. Kennedy, J.C. Mackie, A DFT study on the self-coupling reactions of the three isomeric semiquinone radicals, J. Mol. Struct.: THEOCHEM 958 (2010) 106–115.
[41] P. Du, J. Wang, G. Sun, L. Chen, W. Liu, Hydrogen atom abstraction mechanism for organic compound oxidation by acetylperoxyl radical in Co(II)/peracetic acid activation system, Water Res. 212 (2022) 118113.
[42] H. Bialk, J. Pedersen, NMR investigation of enzymatic coupling of sulfonamide antimicrobials with humic substances, Environ. Sci. Technol. 42 (2008) 106–112.
[43] C. Zhong, H. Cao, Q. Huang, Y. Xie, H. Zhao, Degradation of sulfamethoxazole by Manganese(IV) oxide in the presence of humic acid: role of stabilized semiquinone radicals, Environ. Sci. Technol. 57 (2023) 13625–13634.
[44] T. Chen, H. Dong, Y. Yu, J. Chen, J. Xu, Y. Sun, X. Guan, Neutral phenolic contaminants are not necessarily more resistant to permanganate oxidation than their dissociated counterparts: importance of proton-coupled electron transfer, Environ. Sci. Technol. 57 (2023) 17620–17628.
[45] H. Zhou, S. Zhong, J. Chen, S. Ren, W. Ren, B. Lai, X. Guan, T. Ma, S. Wang, X. Duan, Overlooked complexation and competition effects of phenolic contaminants in a Mn(II)/Nitrilotriacetic acid/peroxymonosulfate system: inhibited generation of primary and secondary high-valent manganese species, Environ. Sci. Technol. 58 (2024) 19080–19089.
[46] P. Shao, S. Yu, X. Duan, L. Yang, H. Shi, L. Ding, J. Tian, L. Yang, X. Luo, S. Wang, Potential difference driving electron transfer via defective carbon nanotubes toward selective oxidation of organic micropollutants, Environ. Sci. Technol. 54 (2020) 8464–8472.
[47] N. Elgrishi, K.J. Rountree, B.D. McCarthy, E.S. Rountree, T.T. Eisenhart, J.L. Dempsey, A practical beginner's guide to cyclic voltammetry, J. Chem. Educ. 95 (2018) 197–206.
[48] A. Jawad, K. Zhan, H. Wang, A. Shahzad, Z. Zeng, J. Wang, X. Zhou, H. Ullah, Z. Chen, Z. Chen, Tuning of persulfate activation from a free radical to a nonradical pathway through the incorporation of non-redox magnesium oxide, Environ. Sci. Technol. 54 (2020) 2476–2488.
[49] C. Hansch, A. Leo, R.W. Taft, A survey of hammett substituent constants and resonance and field parameters, Chem. Rev. 91 (1991) 165–195.
[50] Y. Lee, U. von Gunten, Quantitative structure–activity relationships (QSARs) for the transformation of organic micropollutants during oxidative water treatment, Water Res. 46 (2012) 6177–6195.
[51] J. Peng, P. Zhou, H. Zhou, B. Huang, M. Sun, C.-S. He, H. Zhang, Z. Ao, W. Liu, B. Lai, Removal of phenols by highly active periodate on carbon nanotubes: a mechanistic investigation, Environ. Sci. Technol. 57 (2023) 10804–10815.
[52] J. Wang, M. Zheng, E. Du, W. Chu, H. Guo, A novel source of radicals from UV/Dichloroisocyanurate for surpassing abatement of emerging contaminants versus conventional UV/Chlor(am)ine processes, Environ. Sci. Technol. 57 (2023) 18452–18461.